BIOCHEMISTRY
including biophysical chemistry & molecular biology

Article

pubs.acs.org/biochemistry

Conversion of a Dodecahedral Protein Capsid into Pentamers via Minimal Point Mutations

Hsiao-Nung Chen and Kenneth J. Woycechowsky*

Department of Chemistry, University of Utah, 315 South 1400 East, Salt Lake City, Utah 84112, United States

Supporting Information

ABSTRACT: Protein self-assembly relies upon the formation of stabilizing noncovalent interactions across subunit interfaces. Identifying the determinants of self-assembly is crucial for understanding structure−function relationships in symmetric protein complexes and for engineering responsive nanoscale architectures for applications in medicine and biotechnology. Lumazine synthases (LS's) comprise a protein family that forms diverse quaternary structures, including pentamers and 60-subunit dodecahedral capsids. To improve our understanding of the basis for this difference in assembly, we attempted to convert the capsid-forming LS from *Aquifex aeolicus* (AaLS) into pentamers through a small number of rationally designed amino acid substitutions. Our mutations targeted side chains at ionic (R40), hydrogen bonding (H41), and hydrophobic (L121 and I125) interaction sites along the interfaces between pentamers. We found that substitutions at two or three of these positions could reliably generate pentameric variants of AaLS. Biophysical characterization indicates that this quaternary structure change is not accompanied by substantial changes in secondary or tertiary structure. Interestingly, previous homology-based studies of the assembly determinants in LS's had identified only one of these four positions. The ability to control assembly state in protein capsids such as AaLS could aid efforts in the development of new systems for drug delivery, biocatalysis, or materials synthesis.

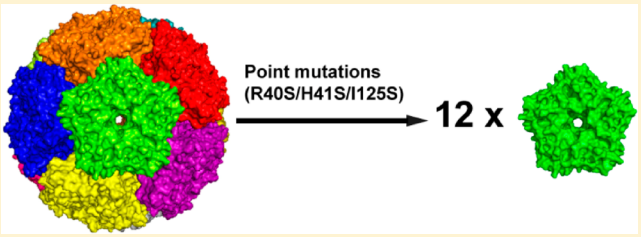

Many proteins form symmetrical, nanoscale architectures from multiple copies of identical polypeptide subunits.[1] These assemblies are held together by noncovalent interactions at the protein−protein interfaces.[2] However, the energetic contributions of individual residues to the stability of protein−protein interfaces are often unevenly distributed.[3,4] Subtle changes can sometimes convert one quaternary structure into another. General rules for predicting quaternary assembly have been slow to emerge.[5−8]

The engineering of nanostructures demands a thorough understanding of the basis for protein self-assembly.[9] In particular, self-assembled protein capsids represent a class of nanoscale scaffolds that holds much promise for various applications, including drug delivery, catalysis, and materials synthesis.[10−13] Indeed, much effort has gone into repurposing capsids to act as containers for a wide variety of non-physiological cargo molecules, such as proteins, nucleic acids, small molecules, and inorganic nanoparticles.[14−23] The controlled and efficient loading of these containers can be facilitated by the ability to interconvert the capsid with lower-order quaternary states.[14,24] Viral capsids possess inherent switches that allow the efficient disassembly and reassembly in response to solution conditions.[25,26] In principle, it should also be possible to engineer the interconversion of quaternary structures between capsids and lower-order assemblies.

The capsid formed by lumazine synthase from *Aquifex aeolicus* (AaLS) is a promising scaffold for engineering novel molecular encapsulation systems.[27−29] AaLS self-assembles into a 60-subunit dodecahedral capsid (Figure 1A) with a diameter of 16 nm, enclosing an empty chamber approximately 9 nm across.[30] This capsid is extremely stable, with a reported melting temperature of 120 °C. While the AaLS capsid presumably assembles from 12 pentamers, lone pentamers of AaLS have never been isolated.

Despite an inability to reversibly disassemble AaLS in vitro, this capsid has been engineered to encapsulate guest proteins in vivo using a charge complementarity strategy.[27,28] In this system, AaLS variants with extra negative charges at the inner surface of the capsid act as hosts for guest proteins bearing a positively charged decaarginine (R_{10}) tag. Encapsulation complexes are formed by coproduction of the AaLS variant and guest protein in *Escherichia coli* cells. Loaded capsids can be purified from these cells but are essentially dead-end complexes. For example, a rationally designed AaLS variant (AaLS-neg) in which four residues at the inner capsid surface have been changed to glutamates can encapsulate R_{10}-tagged green fluorescent protein or HIV protease.[27] Interestingly, the addition of negatively charged residues at the inner surface of the capsid causes a dramatic expansion of the capsid structure, as AaLS-neg forms 180-subunit capsids with a diameter of 28 nm. Directed evolution of AaLS-neg to optimize the encapsulation of R_{10}-tagged HIV protease gave a variant (AaLS-13) with increased negative charge density at the inner

Received: March 19, 2012
Revised: May 10, 2012
Published: May 18, 2012

   dx.doi.org/10.1021/bi3003555 | *Biochemistry* 2012, 51, 4704−4712

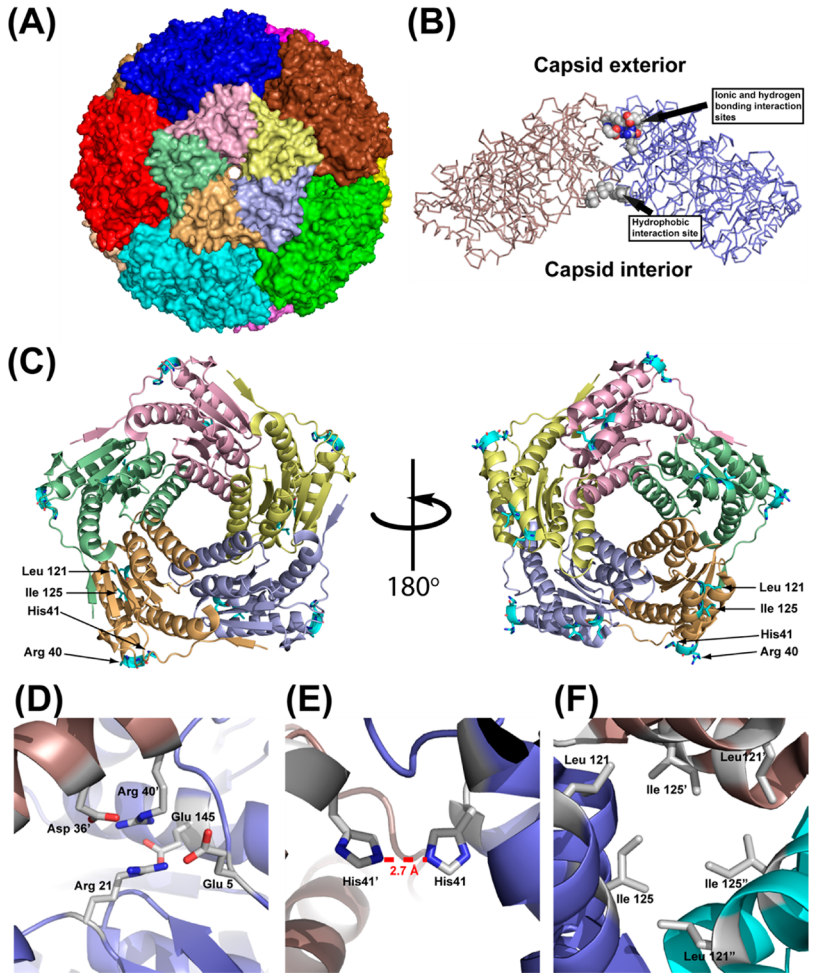

Figure 1. Structure and protein−protein interactions of the AaLS capsid. (A) Surface representation of the AaLS capsid. All of the pentamers are colored differently. In the pentamer at the front of the capsid only, each subunit is colored individually. The rest of the pentamers are colored uniformly. (B) Side view of two adjacent pentamers extracted from the crystal structure of the AaLS capsid. The backbones of the pentamers are colored brown and blue. Residues comprising the ionic, hydrogen bonding, and hydrophobic interaction sites are shown in space-filling representation. (C) Ribbon diagram of a pentamer extracted from the crystal structure of the AaLS capsid. The view on the left is from the outside of the capsid, and the view on the right is from the inside of the capsid. Amino acids that contribute to the ionic, hydrogen bonding, and hydrophobic interaction sites are colored cyan and denoted with arrows. (D) Ionic interaction site. (E) Hydrogen bonding site. (F) Hydrophobic interaction site.

surface that formed capsids 35 nm in diameter, more than twice the size of wild-type AaLS.[28] When produced in the absence of the HIV protease guest, AaLS-13 is isolated a mixture of intact capsids and capsid fragments. These fragments can assemble into capsids in the presence of positively charged guest protein.[29] These observations suggest that it should be feasible to tip the balance between different assembly states of AaLS in a controlled fashion.

In Nature, the lumazine synthase (LS) family of proteins is rich in quaternary structural diversity. In addition to 60-subunit capsids, many homologues form pentamers.[31,32] Decamers that assemble via the dimerization of pentamers have also been observed.[33] Various explanations for what determines the extent of assembly, in particular capsid versus pentamer, have been put forward on the basis of homology. For example, phylogenetic and structural analysis led to the identification of eight sequence positions that have different patterns of conservation between capsid-forming and pentameric LS's.[34] Structural comparisons have also highlighted potential suspects responsible for determining the extent of assembly. Persson et al.[32] purported that a proline residue near the N-terminus of pentameric LS's could prevent capsid formation by breaking a β-strand that aligns with a β-sheet of an adjacent subunit in capsid-forming LS's. Alternatively, Braden et al.[35] suggested that the presence of a five-residue kink in the C-terminal helix is important for capsid formation. In addition, it was also proposed that a four-residue insertion in the loop connecting the fourth and fifth α-helices of a pentameric LS could be responsible for preventing further assembly.[31] This latter hypothesis was tested experimentally by making the insertion in AaLS.[36] The resulting variant still formed capsids, albeit with an expanded structure.

Here, we aimed to identify structural determinants of capsid formation in AaLS by targeted mutation of residues that define the pentamer−pentamer interfaces of the capsid. Using visual inspection of the available high-resolution crystal structure, we identified specific noncovalent interactions between side chains on adjacent pentamers in the AaLS capsid. These interactions were disrupted by strategic amino acid substitutions, effectively preventing capsid formation by halting assembly at the pentamer stage.

dx.doi.org/10.1021/bi3003555 | *Biochemistry* 2012, 51, 4704−4712

MATERIALS AND METHODS

Materials. Cell culture media, salts, and chemical reagents were purchased from Sigma-Aldrich, Fisher Scientific, Pierce Biotechnology, or Bio-Rad (unless otherwise noted) and used without further purification. *Pfu*-turbo DNA polymerase and *E. coli* strains BL21 DE3 and XL1-Blue were purchased from Stratagene. DpnI endonuclease was purchased from New England Biolabs. The oligonucleotides used in this study were synthesized by the DNA/peptide synthesis core facility at the University of Utah.

Site-Directed Mutagenesis. Plasmid pMG-AaLS,[27] encoding the wild-type AaLS gene with an eight-amino acid extension (LEHHHHHH) at the C-terminus, was a kind gift from D. Hilvert (ETH Zürich, Zürich, Switzerland). To avoid potential assembly artifacts, we removed the His tag by mutating the first two histidine codons to stop codons. Using the pMG-AaLS plasmid as the template DNA, site-directed mutagenesis polymerase chain reaction (PCR) was conducted with mutagenic primers HCN61 and HCN62 (Table S1 of the Supporting Information). The PCR mixture (50 μL) was prepared by combining 35 μL of water, 5 μL of 10× reaction buffer, 1 μL of *Pfu*-turbo DNA polymerase (2.5 units/μL), 5 μL of dNTPs (2 mM each), 1 μL of template DNA (10 ng/μL), and 1.5 μL each of forward and reverse primers (10 μM each). During the mutagenesis reaction, temperature cycling was performed in a Mastercycler personal thermocycler (Eppendorf). The *Pfu*-turbo DNA polymerase was activated at 95 °C for 1 min before the temperature cycling was begun. The mutagenesis reaction involved 20 cycles of denaturation (95 °C for 30 s), annealing (55 °C for 30 s), and primer extension (72 °C for 6 min). Following the last cycle, the reaction mixture was incubated for an additional 10 min, to let the DNA polymerase finish the final elongation, before being cooled to 37 °C. The restriction endonuclease DpnI (20 units) was then added to the reaction mixture, which was incubated for an additional 60 min to remove the original DNA template. The mutagenesis reaction product was transformed into $CaCl_2$ competent XL1-Blue cells by heat shock (42 °C for 1 min). The transformed cells were plated onto LB-agar containing ampicillin (100 μg/mL) and incubated overnight at 37 °C. The resulting colonies were used to obtain stocks of plasmid DNA with a QIAprep Spin Miniprep Kit (Qiagen) according to the manufacturer's instructions. The coding portion of the resulting plasmid (pMG-AaLSNoHis) was confirmed by DNA sequencing (University of Utah DNA sequencing core facility).

Additional mutations in the coding region of pMG-AaLSNoHis were also generated by the procedure described above. For these mutagenesis reactions, pMG-AaLsNoHis served as the DNA template. The mutagenic primers used in these reactions are listed in Table S1 of the Supporting Information.

Protein Production and Purification. For producing AaLS variant proteins, $CaCl_2$ competent BL21 DE3 *E. coli* cells were transformed with the pMG-AaLSNoHis plasmid containing the desired mutations. The cells were cultured in 500 mL of LB medium with ampicillin (100 mg/L) at 37 °C and 250 rpm until the OD_{600} reached 0.7. At this point, protein overproduction was induced by the addition of IPTG (final concentration of 0.1 mM). Following incubation for an additional 20 h at 30 °C and 250 rpm, the cells were harvested by centrifugation (5000*g* for 10 min at 4 °C). The cell pellets were resuspended in 10 mL of lysis buffer [50 mM sodium phosphate and 300 mM NaCl (pH 8.0)]. The cells were lysed by incubation with lysozyme (5 mg), RNase A (0.6 mg), and DNase I (10 units) on ice for 30 min followed by sonication. The cell lysate was cleared by centrifugation (8000*g* for 30 min at 4 °C). The cleared lysate (10 mL) was then combined with a saturated ammonium sulfate solution (5 mL), and this mixture was incubated at room temperature for 30 min. Precipitated impurities were removed by centrifugation (8000*g* for 30 min at 4 °C). The supernatant was then dialyzed at 4 °C in ion-exchange buffer A [50 mM sodium phosphate and 20 mM NaCl (pH 8.0)] and then loaded onto an ÄKTA FPLC system (GE Healthcare) equipped with an anion-exchange column (MonoQ 5/50 GL) that was equilibrated with ion-exchange buffer A. Protein was eluted with a gradient from 0 to 100% ion-exchange buffer B [50 mM sodium phosphate and 1 M NaCl (pH 8.0)] over 40 mL at 4 °C. The purity of the protein was analyzed by sodium dodecyl sulfate−polyacrylamide gel electrophoresis. The yields of purified proteins ranged from 30 to 40 mg of protein/L of cell culture.

Size-Exclusion Chromatography (SEC). The approximate sizes of the AaLS variants were analyzed by SEC using an ÄKTA FPLC system equipped with HiPrep 16/60 Sephacryl S-300HR and S-400HR columns (GE Healthcare). The running buffer contained sodium phosphate (50 mM), NaCl (200 mM), and EDTA (5 mM) at pH 8.0. The flow rate was 0.5 mL/min, and the running temperature was 4 °C. Assembly states of the variants were determined on the basis of a comparison to wild-type AaLS (a 1100 kDa, 60-subunit capsid), *Saccharomyces cerevisae* LS (a 98 kDa pentamer),[37] and AaLS-neg (a 3300 kDa, 180-subunit capsid).[27]

In all cases, the protein purified using the procedure described above gave two peaks: one containing an AaLS variant and one containing an impurity. The peak containing the impurity always eluted late relative to the peak of the AaLS variant. This impurity is not stained by Coomassie blue and displayed a high A_{260}/A_{280} ratio. Therefore, the impurity peak probably does not contain protein but may be a nucleic acid contaminant. To check whether this contaminant might influence assembly, proteins were re-injected onto the S-400HR column. The position and shape of the protein peak were unchanged in all cases. All further analyses of the AaLS variants used protein that had been run over the S-400HR column to remove the nucleic acid contaminant.

Sedimentation Equilibrium. Sedimentation equilibrium experiments were performed on a Beckman XL-A analytical ultracentrifuge equipped with an An60Ti rotor and photoelectric scanner. The protein samples were dialyzed into buffer containing sodium phosphate (50 mM), NaCl (200 mM), and EDTA (5 mM) at pH 8.0. Three 160 μL protein samples (130−500 μg/mL) were separately loaded onto three channels of a six-channel centerpiece, and the other channels were loaded with buffer as a reference. Protein samples were spun at speeds ranging from 12500 to 20000 rpm (except for wild-type AaLS, which was spun at 4000 and 5000 rpm) at 20 °C. Once equilibrium at a given speed had been reached, the UV absorbance at 280 nm was measured with a step size of 0.001 cm and 10 averages. The obtained data were analyzed using Ultrascan (University of Texas Health Science Center) and fit to a single-ideal species model (eq 1)

$$A = \exp\{[\ln(A_0) + M\omega^2(1 - \bar{v}\rho)(x^2 - x_0^2)]/2RT\} + B \quad (1)$$

where A is the absorbance at radius x, A_0 is the absorbance at a reference radius x_0, M is the molecular weight of a single species, $\overline{v}$ is the partial specific volume of the protein, ρ is the density of the buffer, ω is the angular velocity of the rotor, R is the universal gas constant, T is the absolute temperature, and B is the baseline correction factor. The values of $\overline{v}$ and ρ at 20 °C were calculated using Sednterp.

Circular Dichroism (CD) Spectroscopy. The CD spectroscopy experiments were performed on a Jasco J-815 spectropolarimeter. The protein samples were dialyzed into buffer containing sodium phosphate (50 mM) and NaCl (200 mM) at pH 8.0 and 4 °C. Far-UV CD spectra of AaLS variants (4 μM) were recorded in a 1 cm path length cuvette at 25 °C by averaging 10 wavelength scans from 200 to 260 nm in 0.1 nm steps with a signal averaging time of 1 s and a bandwidth of 1 nm. Near-UV CD spectra of AaLS variants (160 μM) were recorded in a 1 cm path length cuvette at 25 °C by averaging 10 wavelength scans from 260 to 320 nm in 0.1 nm steps with a signal averaging time of 1 s and a bandwidth of 1 nm. Thermal denaturation curves of AaLS variants (5 μM) were obtained by measuring the ellipticity at 220 nm in a 1 cm path length cuvette from 25 to 95 °C in 0.5 °C intervals with a scan rate of 0.1 °C/min and a signal averaging time of 1 s.

RESULTS

Design of AaLS Variants. The AaLS capsid can be viewed as a dodecamer of pentamers (Figure 1A). The hierarchical assembly of the capsid from pentameric building blocks is further supported by the observation that the assembly of some homologues halts at the pentamer stage.[31,32] To understand the determinants of capsid formation in AaLS, we examined the interface between pentamers in the available crystal structure (Protein Data Bank entry 1hqk).[30] Three distinct types of interaction sites (hydrogen bonding, ionic network, and hydrophobic cluster) that presumably hold the pentamers together in the capsid are found (Figure 1B–F).

The hydrogen bonding interaction found at the 2-fold symmetry axis of the capsid is formed by two histidine residues, H41 and H41′, from two adjacent pentamers (Figure 1E). The length of this hydrogen bond is 2.7 Å, which marks the point of closest approach between two pentamers. The ionic network, located next to the 2-fold symmetry axis, is highly conserved in dodecahedral lumazine synthases and has been previously reported to play an important role in AaLS capsid stability.[36] Two arginine residues, R21 and R40′, from two different pentamers lie at the center of this network (Figure 1D). Their guanidino side chains are stacked on top of each other at a distance of 3.3 Å and are surrounded by acidic residues E5, E145, and D36′. The third pentamer interaction site involves residues L121 and I125, which form a hydrophobic cluster at the 3-fold symmetry axis near the inner surface of the capsids (Figure 1F).

We hypothesized that we could change the AaLS assembly state from a 60-subunit capsid to a pentamer by mutating a subset of the residues listed above. To test this hypothesis, we designed a series of AaLS variants to achieve the targeted disruption of the noncovalent interactions at the interface between pentamers in the wild-type AaLS capsid. Among the amino acids listed above, we focused on five amino acids (R21, R40, H41, L121, and I125) in particular. Substituting negatively charged glutamates in place of these amino acids should both abolish stabilizing interactions and introduce charge–charge repulsion at the native pentamer–pentamer interface. Alternatively, introducing arginine residues at some of these positions could achieve the same effect while also potentially generating steric clashes.

Screening Assembly State by SEC. A series of AaLS variants containing point mutations designed to prevent the formation of stabilizing noncovalent interactions between pentamers were produced in BL21 DE3 *E. coli* cells and purified by ammonium sulfate precipitation followed by anion-exchange chromatography. The assembly states of these AaLS variants were estimated by SEC with a Sephacryl S-400HR column (Table 1 and Table S2 of the Supporting Information).

Table 1. Assembly States of AaLS Variants

protein	no. of pentamers[a]
wild-type AaLS	12
wild-type ScLS	1
R40E/H41E-AaLS	12
R21E/R40E/H41E-AaLS	12
L121E/I125E-AaLS	36[b]
R40E/L121E/I125E-AaLS	2 or 3[c]
H41E/L121E/I125E-AaLS	2 or 3[c]
H41R/L121R-AaLS	1
R40E/H41E/L121E-AaLS	1
R40E/H41E/I125E-AaLS	1
R40S/H41S/I125S-AaLS	1
R40S/H41L/L121E-AaLS	1

[a]Determined by SEC using a Sephacryl S-400HR column. The number of pentamers is defined as the total number of protein subunits divided by 5. [b]This protein eluted like AaLS-neg, which forms a 180-subunit capsid. Thus, this variant probably assembles from 12 pentamers and 20 hexamers, rather than from 36 pentamers. [c]These proteins eluted at volumes between those expected for a dimer of pentamers and a trimer of pentamers.

As suggested by our AaLS capsid structure analysis, R40, H41, L121, and I125 all contribute to capsid assembly. Indeed, simultaneous mutation of the ionic, hydrogen bonding, and hydrophobic interaction sites (R40E/H41E/L121E and R40E/H41E/I125E) appeared to give stable pentamers (Figure 2).

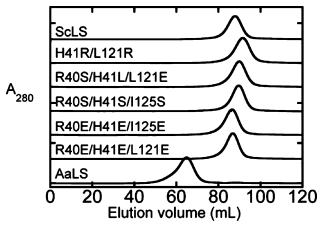

Figure 2. SEC elution profiles of the AaLS variants. Proteins were injected onto a Sephacryl S-400HR column. AaLS (bottom trace) and ScLS (top trace) are standards representing the 60-subunit capsid and pentamer, respectively.

Mutating just the ionic and hydrogen bonding sites (R40E/H41E and R21E/R40E/H41E) has no effect on capsid assembly. Interestingly, changing both residues at the hydrophobic site (L121E/I125E) causes the capsid to expand, which may reflect partial destabilization. This expanded capsid species could contain 180 subunits, as has been seen in other variants of AaLS.[27,36] On the other hand, simultaneous disruption of either the ionic and hydrophobic interactions (R40E/L121E/I125E) or the hydrogen bonding and hydrophobic sites

dx.doi.org/10.1021/bi3003555 | *Biochemistry* 2012, 51, 4704–4712

(H41E/L121E/I125E) is sufficient to hinder capsid formation, but these variants still assemble beyond the pentamer stage, perhaps forming dimers of pentamers or trimers of pentamers. Introducing arginines instead of glutamates at the hydrogen bonding and hydrophobic sites seems to fully prevent any higher-order assembly of the pentamers (Figure 2). Indeed, the H41R/L121R variant might possess the minimal set of mutations sufficient to convert the AaLS capsid to pentamers.

To check for the role of charge repulsion in preventing capsid assembly, we made the R40S/H41S/I125S variant. SEC analysis showed an elution profile similar to that of the analogous R40E/H41E/I125E variant (Figure 2), indicating that the introduction of extra Coulombic repulsion at these positions is not necessary to keep the pentamers from coming together.

The AaLS variants described above were designed without consideration of sequence homology. Nonetheless, an amino acid sequence alignment of AaLS with its pentameric homologue from *Saccharomyces cerevisiae* (ScLS) reveals differences at positions 40, 41, and 121 (Figure S1 of the Supporting Information). Therefore, we made the R40S/H41L/L121E variant of AaLS in which the amino acids at these positions correspond to those found in ScLS. This variant and ScLS exhibit similar elution profiles as determined by SEC (Figure 2), suggesting that these positions may have been important in the evolution of LS quaternary structure.

The pentameric variants identified above by SEC with the S-400HR column were also injected onto an S-300HR column, which has an optimal size separation range for smaller proteins versus that of the S-400HR column. The elution profiles from the S-300HR column exhibited trends similar to those from the S-400HR column (Table S2 of the Supporting Information).

Sedimentation Equilibrium Studies. SEC is a low-resolution method for determining quaternary structure. While the results described above unambiguously show a shift to a much lower assembly state for some of the AaLS variants, our designation of the slowest-eluting variants as pentamers was somewhat tentative. Therefore, we turned to sedimentation equilibrium experiments to confirm the subunit stoichiometries. For all variants, the sedimentation equilibrium data fit well to a single-ideal species model and gave predicted masses close to that calculated for the pentamer (Table 2, Figure 3, and Figure S2 of the Supporting Information).

Assessing the Folding and Stability of AaLS Variants. To determine whether the dramatic changes in quaternary structure were accompanied by large changes in folding and stability, we utilized CD spectroscopy. LS is a member of the α and β (α/β) class of protein structure. Far-UV CD spectra were obtained to compare the secondary structure content of the AaLS variants. All of the spectra displayed broad minima between 222 and 208 nm, typical of an α/β protein (Figure 4A). The similar shapes of the spectra for wild-type AaLS and all of the variants indicate that none of the mutations induced major changes in overall secondary structure. The H41R/L121R-AaLS and R40E/H41E/I125E-AaLS variants had the lowest signal intensities (~12−16% less negative θ values than wild-type AaLS between 220 and 208 nm), but these differences are likely within the scatter of the experiment (Figure S3 of the Supporting Information). Thus, the secondary structure contents of the variants are all similar to that of wild-type AaLS.

The tertiary structures of the AaLS variants were examined by near-UV CD spectroscopy, which reports on the environment around two tyrosines and two tryptophans in each protein. Only minor deviations were observed between the spectra, consistent with preservation of the overall fold (Figure 4B). These differences may stem from perturbations around W137, which lies near the pentamer interface in the wild-type AaLS capsid.

Table 2. Assembly States of AaLS Variants Determined by Sedimentation Equilibrium Analysis

protein	pentameric molecular mass (kDa)[a]	observed molecular mass (kDa)[b]
wild-type AaLS	N/A[c]	970[c]
wild-type ScLS	98	92
R40S/H41S/I125S-AaLS	84	79
R40E/H41E/I125E-AaLS	85	85
R40E/H41E/L121E-AaLS	85	81
H41R/L121R-AaLS	85	82

[a]Pentameric molecular masses were obtained by calculating the monomeric molecular mass from the amino acid sequence and multiplying by 5. [b]Observed molecular masses were determined by fitting the data from sedimentation equilibrium experiments to a single-ideal species model. [c]Not applicable. Wild-type AaLS forms a 60-subunit capsid with a molecular mass of 1000 kDa.

Wild-type AaLS is exceptionally thermostable with a reported melting temperature of 120 °C.[30] The extent to which the pentamer interfaces contribute to the stability is not known. Therefore, we obtained thermal unfolding curves by monitoring the ellipticity at 220 nm with an increasing temperature (Figure 4C). Consistent with its reported stability, wild-type AaLS showed little change in signal up to 95 °C. In contrast, the midpoint of the unfolding transition for mesophilic ScLS occurred around 56 °C, which is close to the reported value.[37] All of the pentameric AaLS variants show signs of a partial unfolding transition before 95 °C but remain fully folded up to 80 °C. For R40S/H41S/I125S-AaLS and R40S/H41L/L121E-AaLS, the transitions are incomplete at 95 °C. H41R/L121R-AaLS, R40E/H41E/L121E-AaLS, and R40E/H41E/I125E-AaLS retained a substantial amount of CD signal following the ends of their transitions. The structural basis of this residual signal is not clear but may indicate a complex unfolding mechanism. To further investigate the thermal denaturation behavior of the proteins, we performed additional measurements in 4 M urea. The far-UV spectra were similar for wild-type AaLS and the three variants, and the partial unfolding transitions of the variants occurred at lower temperatures (Figure S4A,B of the Supporting Information). Although the magnitudes of the signal changes in the melting curves are somewhat different in 4 M urea relative to 0 M urea (Figure 4C and Figure S4B of the Supporting Information), there is still no evidence of a second transition for these variants up to 99 °C. In contrast to the variants, wild-type AaLS shows very little change in signal between 10 and 99 °C in 4 M urea. To further destabilize the proteins, we obtained far-UV CD spectra in 8 M urea. Under this condition, the three variants seem to be fully unfolded at 10 °C and wild-type AaLS seems to maintain a high degree of structure (Figure S4C of the Supporting Information). Interestingly, wild-type AaLS in 8 M urea does not begin to unfold until the temperature reaches ~85 °C, at which point the CD signal intensity slowly and continuously decreases (Figure S4D of the Supporting Information).

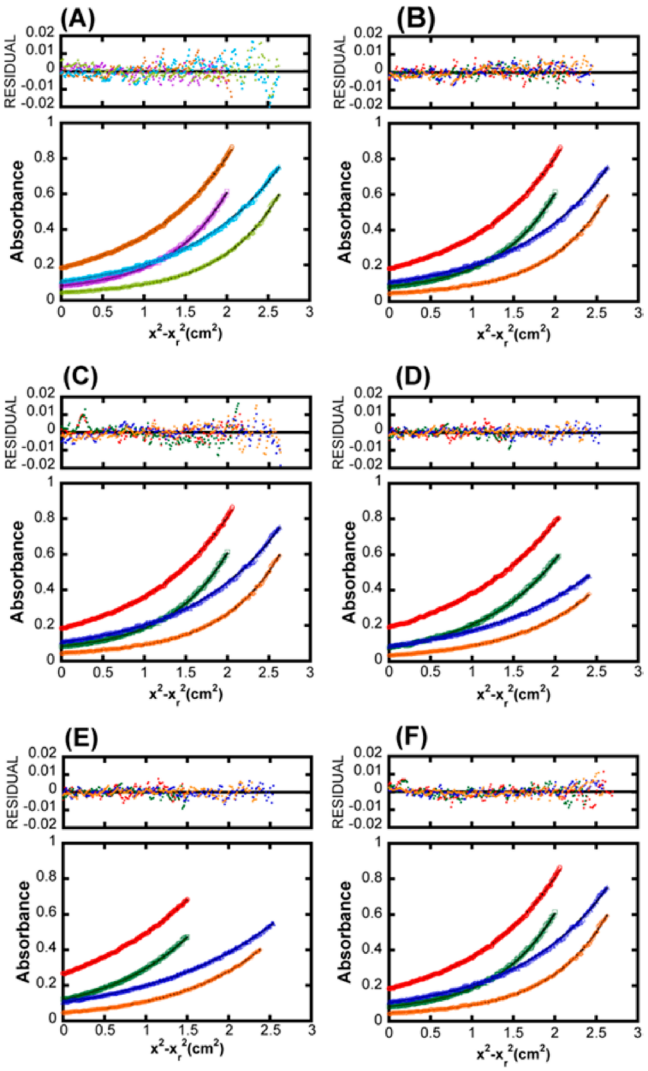

Figure 3. Plots of sedimentation equilibrium data. All samples were spun at two different concentrations (0.50 and 0.25 mg/mL). (A) Wild-type AaLS was spun at 4000 rpm (brown and light blue for 0.50 and 0.25 mg/mL samples, respectively) and 5000 rpm (purple and light green for 0.50 and 0.25 mg/mL samples, respectively). (B–F) Samples were spun at 12500 rpm (red and blue for 0.50 and 0.25 mg/mL samples, respectively) and 15000 rpm (green and orange for 0.50 and 0.25 mg/mL samples, respectively): (B) wild-type ScLS, (C) R40E/H41E/L121E-AaLS, (D) R40E/H41E/I125E-AaLS, (E) R40S/H41S/I125S-AaLS, and (F) H41R/L121R-AaLS. Black curves represent ideal curves derived from fitting the data to a single-ideal species model in all cases. Residuals for each data set are shown above the absorbance plots.

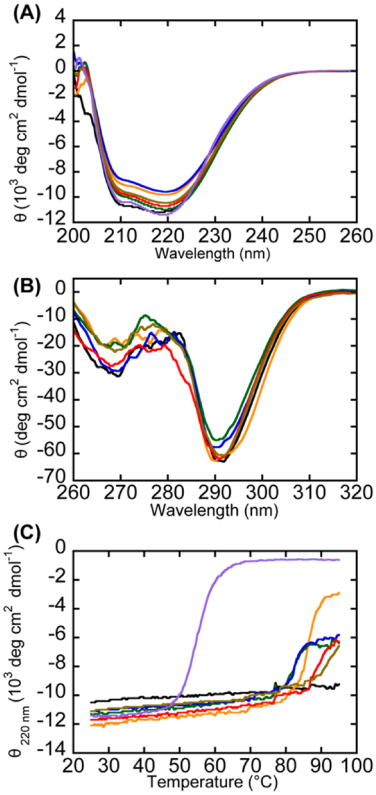

Figure 4. Analysis of protein structure and stability by CD spectroscopy. (A) Far-UV CD spectra. (B) Near-UV-CD spectra. (C) Thermal unfolding curves. Proteins analyzed in panels A–C were wild-type AaLS (black), ScLS (purple), R40S/H41S/I125S-AaLS (red), R40E/H41E/I125E-AaLS (blue), R40E/H41E/L121E-AaLS (green), R40S/H41L/L121E-AaLS (brown), and H41R/L121R-AaLS (orange).

However, this transition is still not complete at 99 °C. Nonetheless, these data unequivocally show that the loss of the pentamer interfaces in AaLS is accompanied by a significant decrease in stability, but that the pentameric variants retain a high degree of thermostability. Further study will be required to understand the unfolding mechanisms of wild-type AaLS and its variants.

DISCUSSION

The conversion of protein assemblies into independently folded building blocks by targeted disruption of noncovalent interactions at subunit interfaces has a long track record of success. For example, the tetramer of rabbit fructose 1,6-bisphosphate aldolase was converted to either dimers or monomers by one or two point mutations at interface residues.[38,39] Similarly, a single lysine to glutamate mutation was sufficient to convert the normally tetradecameric *E. coli* chaperonin GroEL to monomers.[40] In addition, human arginase has been converted from a trimer to monomers by a glutamate to glutamine substitution that broke an ionic interaction at the 3-fold symmetry axis.[41] The dimeric tyrosyl tRNA synthetase from *Bacillus stearothermophilus* provides another interesting case in which the substitution of aspartate for phenylalanine at the 2-fold symmetry axis generated a pH-dependent reversible switch for dimer assembly.[42] These examples demonstrate that one or a few mutations that remove noncovalent interactions between subunits (or that introduce new destabilizing interactions at the subunit interface) are often sufficient to change quaternary structure without substantially altering secondary or tertiary structure. However, the loss of protein–protein interfaces is accompanied by a loss of stability in these variants. In the examples above, the symmetry axes of the wild-type complexes proved to be rich sources for designing variants that still fold but do not fully assemble. These principles held true in our pentameric AaLS variants in which both the 2- and 3-fold symmetry axes of the wild-type capsid were targeted for mutation. These variants also showed signs of lower stability but still folded and retained a great deal of thermostability.

For many large oligomeric proteins, assembly is believed to be a hierarchical process in which monomers first independently assemble to form a lower-order quaternary state and these

dx.doi.org/10.1021/bi3003555 | *Biochemistry* 2012, 51, 4704–4712

partially assembled building blocks further associate to form the final higher-order structure.[43] For AaLS, the 60-subunit capsid is believed to assemble from 12 pentameric building blocks.[30] We were able to halt assembly at the pentamer stage by introducing two or three point mutations. The trapping of presumed assembly intermediates by rationally designed point mutations has also been accomplished for other proteins. For example, inorganic pyrophosphatase from *E. coli* was converted from a hexamer to trimers by simultaneously mutating two histidines to glutamines at the 2-fold symmetric interface of the hexamer.[44] In another case, two mutations (tryptophan to alanine and methionine to alanine) were used to isolate the hexameric form of HIV capsid protein.[45] The inability of these hexamers to further assemble was ascribed to the removal of a hydrophobic interaction at the 2-fold symmetry axis between hexameric building blocks of the wild-type capsid. Of particular relevance to our study, the assembly states of both maxi- and mini-ferritins were simplified by minimal point mutations. For maxi-ferritin (bacterioferritin from *E. coli*), the 24-subunit capsid was converted to folded dimers by several different single-amino acid substitutions at the 2- and 3-fold symmetry axes.[46] For mini-ferritin (*E. coli* DNA binding protein from starved cells), two mutations at the 3-fold symmetry axis led to dimers rather than 12-subunit capsids.[47] In these studies, wild-type residues were replaced with alanines to remove stabilizing electrostatic interactions at subunit interfaces. Thus, the strategy of simplifying complex quaternary structures by mutating residues at symmetry axes between building blocks may be broadly applicable.

A definitive understanding of assembly state determinants in LSs has remained elusive. Previous attempts to design disruptions in the interactions between pentamers of capsid-forming LSs gave rise to interesting changes in capsid structure rather than preventing further assembly of pentamers.[36] By visual inspection of the AaLS capsid structure, we identified a set of amino acid side chains that formed stabilizing interactions between pentamers.

By mutating subsets of these residues, we induced quaternary structure changes in AaLS. Simultaneous disruption of the ionic, hydrogen bonding, and hydrophobic interaction sites reliably yields stable pentamers. Interestingly, introduction of negatively charged residues at the hydrophobic site alone led to an expansion of the capsid. Presumably, the larger capsid size helps to minimize Coulombic repulsion in the variant, perhaps by increasing the size of the pore at the 3-fold symmetry axis. Because the stabilizing effects of individual protein−protein interactions are multiplied by the symmetry of the capsid,[1] it is perhaps unsurprising that the interfaces are highly plastic and resilient to localized disruptions. Indeed, a similar capsid expansion was found to relieve steric clashes at the pentamer−pentamer interface in AaLS upon insertion of a four-amino acid loop between amino acids 129 and 130 (vide infra).[36] Mutation of only two of the three interaction sites was often sufficient to break the capsid but did not always completely abolish associations between pentamers. Although a more detailed characterization would be required to assign the precise assembly states of the R40E/L121E/I125E-AaLS and H41E/L121E/I125E-AaLS variants, SEC analysis indicates that they form either dimers of pentamers or trimers of pentamers. The lumazine synthase from *Brucella abortus* (BaLS) provides a natural precedent for a pentamer dimer, in which 10 total subunits assemble into a D_5-symmetric complex. The pentamer−pentamer interface of BaLS involves π-stacking between F121 of one pentamer and H124 and F128 of the other pentamer (using the numbering of Ainciart et al.[33]). Intriguingly, these residues correspond to L121, R127, and an insertion proximal to K131 of AaLS, respectively, based on their amino acid sequence alignment. It is tempting to speculate that a pentamer dimer of AaLS variants might arise from a salt bridge between the newly introduced glutamate at position 121 and the positively charged residues at positions 127 and 131. A D_5-symmetric assembly would lead to the formation of 10 such salt bridges (one per subunit) distributed over this new interface, which could provide substantial stabilization. It is difficult to envision what a trimer of pentamers might look like, given the requirements of symmetric assembly;[1] any arrangement of three pentamers is likely to possess open sites for the binding of more pentamers via interactions equivalent to those in the initial trimer of pentamers. However, it is worth noting that a variant of ScLS, in which three arginines were introduced at the 5-fold symmetry axis, has been reported to undergo a dynamic exchange between a pentamer and a trimer of pentamers.[37] Altogether, the quaternary structures of the variants reported here implicate residues R40, H41, L121, and I125 as important contributors to capsid assembly.

It should be noted that these sequence positions may not be the sole determinants of AaLS capsid assembly. For example, R21 may play a role comparable to that of R40 in stabilizing the capsid, as part of the ionic network (Figure 1B). Additional residues that we did not consider in our designs might also act as determinants of capsid assembly.

A previous study by Fornsari et al.[34] used sequence and structural analysis to identify a set of eight amino acids (G6, N23, D36, I125, E126, G129, K131, and E145) responsible for capsid formation by LS's. Interestingly, only one of these eight sequence positions (I125) was changed in our pentameric variants, and some of our pentameric variants did not have changes at any of these eight sequence positions. While this previous study did not include AaLS, its homology with other capsid-forming LS's suggests that our findings are relevant across this family. Of the seven positions that we did not mutate, our analysis of the noncovalent interactions between pentamers in wild-type AaLS also identified D36 and E145 as part of an ionic network (Figure 1E). The main chain of G6 contributes a hydrogen bond to the ionic network, which may also be significant for capsid assembly. E126 lies next to L121′ on the neighboring pentamer, and a contact between C_γ of E126 and C_δ of L121′ may help stabilize the hydrophobic cluster. G129 makes a main chain−main chain hydrogen bond with A25′; mutation of this amino acid could also potentially hinder association of pentamers by disrupting this favorable interaction and/or introducing unfavorable steric clashes. N23 is in the proximity of an adjacent pentamer, and its side chain carbonyl oxygen may form a stabilizing $n \rightarrow \pi^*$ interaction[48] with the backbone carbonyl carbon of T130′. In the AaLS crystal structure, K131 does not appear to make close contacts with any other residue and projects to the capsid interior.

The first 10 N-terminal residues have also been proposed to act as determinants of capsid formation,[32] based on whether this region can extend a β-sheet from an adjacent subunit within the same pentamer. Our findings suggest an alternative role for the N-terminus in stabilizing the ionic network through proper positioning of E5 and G6. A kink in the C-terminal α-helix with a sequence motif of G(T/G)K(A/H)GN at positions 129 to 134 has also been identified as a likely determinant of capsid assembly.[35,49] This motif includes G129 and K131 from

the set of eight amino acids discussed above. Further, pentameric LSs often have insertions of one to four amino acids following G129 that likely hinder capsid formation by introducing steric clashes at the pentamer−pentamer interfaces.[31,34,36] However, insertion of four amino acids into AaLS at this position does not prevent capsid assembly.[36] The expanded structures formed by this insertion variant underscore the plasticity of the protein−protein interfaces in the capsid. Our results suggest that it is not necessary to perturb the structure of the protein in this region to prevent capsid assembly. While these other proposed capsid determinants are not inconsistent with our findings, identifying and verifying additional sets of residues that can convert the capsid into pentamers will require further study.

In addition to advancing a basic understanding of LS capsid assembly, our results may also aid in efforts to utilize this scaffold for bionanotechnology. AaLS has shown much promise as a customizable molecular container.[27,28] The ability to control assembly state would potentially improve the versatility of AaLS-based encapsulation systems. The pentameric variants described herein might provide valuable jumping off points for the design of reversible capsid assembly switches. Controlled assembly and disassembly of the AaLS capsid would allow the loading of cargo molecules in vitro, which could help make AaLS a powerful tool for applications such as drug delivery, catalysis, or the synthesis of nanomaterials.

■ ASSOCIATED CONTENT

Supporting Information

Additional information (sequences, alignments, SEC data, and sedimentation equilibrium plots). This material is available free of charge via the Internet at http://pubs.acs.org.

■ AUTHOR INFORMATION

Corresponding Author

*Department of Chemistry, University of Utah, 315 S. 1400 E., Room 2020, Salt Lake City, UT 84112. Telephone: (801) 587-9973. Fax: (801) 581-8433. E-mail: kwoycech@chem.utah.edu.

Funding

This work was supported by the University of Utah.

Notes

The authors declare no competing financial interest.

■ ACKNOWLEDGMENTS

We thank Debbie Eckert for assistance with the sedimentation equilibrium experiments.

■ ABBREVIATIONS

AaLS, *A. aeolicus* lumazine synthase; CD, circular dichroism; EDTA, ethylenediaminetetraacetic acid; FPLC, fast protein liquid chromatography; IPTG, isopropyl β-D-1-thiogalactopyranoside; LS, lumazine synthase; SEC, size-exclusion chromatography; ScLS, *S. cerevisiae* lumazine synthase.

■ REFERENCES

(1) Goodsell, D. S., and Olson, A. J. (2000) Structural symmetry and protein function. *Annu. Rev. Biophys. Biomol. Struct. 29*, 105−153.

(2) Ali, M. H., and Imperiali, B. (2005) Protein oligomerization: How and why. *Bioorg. Med. Chem. 13*, 5013−5020.

(3) Clackson, T., and Wells, J. A. (1995) A hot spot of binding energy in a hormone-receptor interface. *Science 267*, 383−386.

(4) Moreira, I. S., Fernandes, P. A., and Ramos, M. J. (2007) Hot spots: A review of the protein-protein interface determinant amino acid residues. *Proteins: Struct., Funct., Bioinf. 68*, 803−812.

(5) Janin, J., Bahadur, R. P., and Chakrabarti, P. (2008) Protein-protein interaction and quaternary structure. *Q. Rev. Biophys. 41*, 133−180.

(6) Grueninger, D., Treiber, N., Ziegler, M. O. P., Koetter, J. W. A., Schulze, M.-S., and Schulz, G. E. (2008) Designed protein-protein association. *Science 319*, 206−209.

(7) André, I., Bradley, P., Wang, C., and Baker, D. (2007) Prediction of the structure of symmetrical protein assemblies. *Proc. Natl. Acad. Sci. U.S.A. 104*, 17656−17661.

(8) Padilla, J. E., Colovos, C., and Yeates, T. O. (2001) Nanohedra: Using symmetry to design self assembling protein cages, layers, crystals, and filaments. *Proc. Natl. Acad. Sci. U.S.A. 98*, 2217−2221.

(9) Tsai, C.-J., Zheng, J., Zanuy, D., Haspel, N., Wolfson, H., Alemán, C., and Nussinov, R. (2007) Principles of nanostructure design with protein building blocks. *Proteins: Struct., Funct., Bioinf. 68*, 1−12.

(10) Douglas, T., and Young, M. (2006) Viruses: Making friends with old foes. *Science 312*, 873−875.

(11) Papapostolou, D., and Howorka, S. (2009) Engineering and exploiting protein assemblies in synthetic biology. *Mol. BioSyst. 5*, 723−732.

(12) Bode, S. A., Minten, I. J., Nolte, R. J., and Cornelissen, J. J. (2011) Reactions inside nanoscale protein cages. *Nanoscale 3*, 2376−2389.

(13) Ma, Y., Nolte, R. J., and Cornelissen, J. J. (2012) Virus-based nanocarriers for drug delivery. *Adv. Drug Delivery Rev. 64*, 811−825.

(14) Minten, I. J., Hendriks, L. J., Nolte, R. J., and Cornelissen, J. J. (2009) Controlled encapsulation of multiple proteins in virus capsids. *J. Am. Chem. Soc. 131*, 17771−17773.

(15) Kwak, M., Minten, I. J., Anaya, D. M., Musser, A. J., Brasch, M., Nolte, R. J., Müllen, K., Cornelissen, J. J., and Herrmann, A. (2010) Virus-like particles templated by DNA micelles: A general method for loading virus nanocarriers. *J. Am. Chem. Soc. 132*, 7834−7835.

(16) Fiedler, J. D., Brown, S. D., Lau, J. L., and Finn, M. G. (2010) RNA-directed packaging of enzymes within virus-like particles. *Angew. Chem., Int. Ed. 49*, 9648−9651.

(17) Lau, J. L., Baksh, M. M., Fiedler, J. D., Brown, S. D., Kussrow, A., Bornhop, D. J., Ordoukhanian, P., and Finn, M. G. (2011) Evolution and protein packaging of small-molecule RNA aptamers. *ACS Nano 5*, 7722−7729.

(18) O'Neil, A., Reichhardt, C., Johnson, B., Prevelige, P. E., and Douglas, T. (2011) Genetically programmed in vivo packaging of protein cargo and its controlled release from bacteriophage P22. *Angew. Chem., Int. Ed. 50*, 7425−7428.

(19) Wu, W., Hsiao, S. C., Carrico, Z. M., and Francis, M. B. (2009) Genome-free viral capsids as multivalent carriers for taxol delivery. *Angew. Chem., Int. Ed. 48*, 9493−9497.

(20) Stephanopoulos, N., Tong, G. J., Hsiao, S. C., and Francis, M. B. (2010) Dual-surface modified virus capsids for targeted delivery of photodynamic agents to cancer cells. *ACS Nano 4*, 6014−6020.

(21) Uchida, M., Morris, D. S., Kang, S., Jolley, C. C., Lucon, J., Liepold, L. O., LaFrance, B., Prevelige, P. E. J., and Douglas, T. (2012) Site-directed coordination chemistry with P22 virus-like particles. *Langmuir 28*, 1998−2006.

(22) Aniagyei, S. E., Kennedy, C. J., Stein, B., Willits, D. A., Douglas, T., Young, M. J., De, M., Rotello, V. M., Srisathiyanarayanan, D., Kao, C. C., and Dragnea, B. (2009) Synergistic effects of mutations and nanoparticle templating in the self-assembly of cowpea chlorotic mottle virus capsids. *Nano Lett. 9*, 393−398.

(23) Polanams, J., Ray, A. D., and Watt, R. K. (2005) Nanophase iron phosphate, iron arsenate, iron vanadate, and iron molybdate minerals synthesized within the protein cage of ferritin. *Inorg. Chem. 44*, 3203−3209.

(24) Lu, X., Thompson, J. R., and Perry, K. L. (2012) Encapsidation of DNA, a protein and a fluorophore into virus-like particles by the capsid protein of cucumber mosaic virus. *J. Gen. Virol. 93*, 1120−1126.

(25) Fraenkel-Conrat, H., and Williams, R. C. (1955) Reconstitution of active tobacco mosaic virus from its inactive protein and nucleic acid components. *Proc. Natl. Acad. Sci. U.S.A. 41*, 690−698.
(26) Zhao, X., Fox, J. M., Olson, N. H., Baker, T. S., and Young, M. J. (1995) In vitro assembly of cowpea chlorotic mottle virus from coat protein expressed in *Escherichia coli* and in vitro-transcribed viral cDNA. *Virology 207*, 486−494.
(27) Seebeck, F. P., Woycechowsky, K. J., Zhuang, W., Rabe, J. P., and Hilvert, D. (2006) A simple tagging system for protein encapsulation. *J. Am. Chem. Soc. 128*, 4516−4517.
(28) Wörsdörfer, B., Woycechowsky, K. J., and Hilvert, D. (2011) Directed evolution of a protein container. *Science 331*, 589−592.
(29) Wörsdörfer, B., Pianowski, Z., and Hilvert, D. (2012) Efficient in vitro encapsulation of protein cargo by an engineered protein container. *J. Am. Chem. Soc. 134*, 909−911.
(30) Zhang, X., Meining, W., Fischer, M., Bacher, A., and Ladenstein, R. (2001) X-ray structure analysis and crystallographic refinement of lumazine synthase from the hyperthermophile *Aquifex aeolicus* at 1.6 Å resolution: Determinants of thermostability revealed from structural comparisons. *J. Mol. Biol. 306*, 1099−1114.
(31) Meining, W., Mörtl, S., Fischer, M., Cushman, M., Bacher, A., and Ladenstein, R. (2000) The atomic structure of pentameric lumazine synthase from *Saccharomyces cerevisiae* at 1.85 Å resolution reveals the binding mode of a phosphonate intermediate analogue. *J. Mol. Biol. 299*, 181−197.
(32) Persson, K., Schneider, G., Jordan, D. B., Viitanen, P. V., and Sandalova, T. (1999) Crystal structure analysis of a pentameric fungal and an icosahedral plant lumazine synthase reveals the structural basis for differences in assembly. *Protein Sci. 8*, 2355−2365.
(33) Ainciart, N., Zylberman, V., Craig, P. O., Nygaard, D., Bonomi, H. R., Cauerhff, A. A., and Goldbaum, F. A. (2011) Sensing the dissociation of a polymeric enzyme by means of an engineered intrinsic probe. *Proteins: Struct., Funct., Bioinf. 79*, 1079−1088.
(34) Fornasari, M. S., Laplagne, D. A., Frankel, N., Cauerhff, A. A., Goldbaum, F. A., and Echave, J. (2004) Sequence determinants of quaternary structure in lumazine synthase. *Mol. Biol. Evol. 21*, 97−107.
(35) Braden, B. C., Velikovsky, C. A., Cauerhff, A. A., Polikarpov, I., and Goldbaum, F. A. (2000) Divergence in macomolecular assembly: X-ray crystallographic structure analysis of lumazine synthase from *Brucella arortus*. *J. Mol. Biol. 297*, 1031−1036.
(36) Zhang, X., Konarev, P. V., Petoukhov, M. V., Svergun, D. I., Xing, L., Cheng, R. H., Haase, I., Fischer, M., Bacher, A., Ladenstein, R., and Meining, W. (2006) Multiple assembly states of lumazine synthase: A model relating catalytic function and molecular assembly. *J. Mol. Biol. 362*, 753−770.
(37) Woycechowsky, K. J., Seebeck, F. P., and Hilvert, D. (2006) Tunnel plasticity and quaternary structural integrity of a pentameric protein ring. *Protein Sci. 15*, 1106−1114.
(38) Beernink, P. T., and Tolan, D. R. (1994) Subunit interface mutants of rabbit muscle aldolase form active dimers. *Protein Sci. 3*, 1383−1391.
(39) Beernink, P. T., and Tolan, D. R. (1996) Disruption of aldolase A tetramer into catalytically active monomers. *Proc. Natl. Acad. Sci. U.S.A. 93*, 5374−5379.
(40) Horovitz, A., Bochkareva, E. S., and Girshovich, A. S. (1993) The N terminus of the molecular chaperonin GroEL is a crucial structural element for its assembly. *J. Biol. Chem. 268*, 9957−9959.
(41) Sabio, G., Mora, A., Rangel, M. A., Quesada, A., Marcos, C. F., Alonso, J. C., Soler, G., and Centeno, F. (2001) Glu-256 is a main structural determinant for oligomerisation of human arginase I. *FEBS Lett. 501*, 161−165.
(42) Jones, D. H., McMillan, A. J., and Fersht, A. R. (1985) Reversible dissociation of dimeric tyrosyl-tRNA synthetase by mutagenesis at the subunit interface. *Biochemistry 24*, 5852−5857.
(43) Bahadur, R. P., Rodier, F., and Janin, J. (2007) A dissection of the protein-protein interfaces in icosahedral virus capsids. *J. Mol. Biol. 367*, 574−590.
(44) Velichko, I. S., Mikalahati, K., Kasho, V. N., Dudarenkov, V. Y., Hyytiä, T., Goldman, A., Cooperman, B. S., Lahti, R., and Baykov, A. A. (1998) Trimeric inorganic pyrophosphatase of *Escherichia coli* obtained by directed mutagenesis. *Biochemistry 37*, 734−740.
(45) Pornillos, O., Ganser-Pornillos, B. K., Banumathi, S., Hua, Y., and Yeager, M. (2010) Disulfide bond stabilization of the hexameric capsomer of human immunodeficiency virus. *J. Mol. Biol. 401*, 985−995.
(46) Zhang, Y., Raudah, S., Teo, H., Fan, R., Sun, X., and Orner, B. P. (2010) Alanine-shaving mutagenesis to determine key interfacial residues governing the assembly of a nano-cage maxi-ferritin. *J. Biol. Chem. 285*, 12078−12086.
(47) Zhang, Y., Fu, J., Chee, S. Y., Ang, E. X. W., and Orner, B. P. (2011) Rational disruption of the oligomerization of the mini-ferritin *E. coli* DPS through protein-protein interface mutation. *Protein Sci. 20*, 1907−1917.
(48) Bartlett, G. J., Choudhary, A., Raines, R. T., and Woolfson, D. N. (2010) n→π^* interactions in proteins. *Nat. Chem. Biol. 6*, 615−620.
(49) Gerhardt, S., Haase, I., Steinbacher, S., Kaiser, J. T., Cushman, M., Bacher, A., Huber, R., and Fischer, M. (2002) The structural basis of riboflavin binding to *Schizosaccharomyces pombe* 6,7-dimethyl-8-ribityllumazine synthase. *J. Mol. Biol. 318*, 1317−1329.